








Corrosion behavior of 17 - 4PH steel, produced by the MIM process, sintered in different atmospheres

Otávio Real Cappellaro¹ , Jorge Luis Braz Medeiros¹ , Giovanni Pereira Uva¹ ,
Neftali Lenin Villarreal Carreno² , Guilherme Kurz Maron² , Luciano Volcanoglo Biehl¹ ,
José Henrique Alano¹ 

¹Universidade Federal do Rio Grande, Escola de Engenharia. Rio Grande, RS, Brasil.

²Universidade Federal de Pelotas, Centro de Desenvolvimento Tecnológico. Pelotas, RS, Brasil.

e-mail: jorge.braz@furg.br, otavio.cappellaro@hotmail.com, uvagiovanni16@gmail.com, nef-tali@ufpel.edu.br, g_maron@hotmail.com, lucianobiehl@furg.br, alano.jh@furg.br

ABSTRACT

The Metal Injection Molding (MIM) process is used for small parts, complex geometries, and high production volumes. Among the various ferrous and non-ferrous alloys that use this technology, the precipitation-hardened stainless steel Catamold 17 - 4 PH stands out. This class of steel used in the aerospace and automotive industries is characterized by its resistance to corrosion combined with excellent mechanical properties. The sintering process of this steel is carried out in a controlled hydrogen-based atmosphere, which, together with the raw material, impacts the manufacturing cost of the components. In this work, different sintering atmospheres were evaluated, and the effects were verified using optical microscopy, scanning electron microscopy (SEM), the EDS microprobe, microhardness, and potentiodynamic polarization techniques. The results demonstrated that the microstructure and microhardness of the substrate were not affected. However, deleterious effects were detected with an increase in the level of porosity, compromising the corrosion resistance of the analyzed samples. Comparatively, samples with pure nitrogen showed better corrosion resistance compared to those with the presence of water vapor. However, it was less resistant to corrosion than found in the literature in a hydrogen atmosphere, considered the state of the art for Catamold 17 - 4 PH stainless steel.

Keywords: Metals; MIM; 17 - 4 PH; Corrosion.

1. INTRODUCTION

The high demand for low-cost materials with good mechanical properties and high corrosion resistance promoted numerous studies regarding Precipitation Hardening (PH) Stainless Steels (SS) [1–3]. Based on their microstructures, they can be classified as martensitic, semi-austenitic and austenitic [4, 5]. The 17 - 4 PH SS, also known AISI 630, is one of the most common and versatile martensitic precipitation hardened alloys. Due to their high strength and toughness, as well as good corrosion resistance, they are frequently applied in a wide variety of industries, including aerospace, automotive, marine, nuclear and chemical [6]. The good mechanical properties and corrosion resistance of the 17 - 4 PH SS is attributed to the presence of homogeneously distributed fine precipitates of alloying elements such as chromium, aluminum, titanium, niobium, and copper [6, 7].

Recent reports have described the use of Metal injection moulding (MIM) for the fabrication of complex 17 - 4 PH SS [8–10]. MIM is a metalworking technique that consists in shaping metal particles with the aid of a small quantity of a polymer followed by sintering process, resulting in highly dense materials with complex shape [10]. The MIM process comprises of four well defined stages: the first step is the preparation of the feedstock by mixing the metallic powder with the polymeric binder; the second one is the injection of the as-prepared feedstock into a mould of the required shape; the third stage is the thermal debinding to remove most part of the binder; and finally, the last step consists in a sintering process in a controlled atmosphere to densify the metal power [10–13].

According to the aforementioned characteristics, the fabrication of 17 - 4 PH SS by MIM process becomes an interesting alternative, resulting in a material with high mechanical strength, toughness and good corrosion resistance [14–17]. However, the SS microstructure are directly dependent on process, specially the atmosphere

used during the sintering, where the oxygen content increases the porosity and decreases the relative density of the steel. Therefore, a detailed investigation of the electrochemical behavior of steel corrosion in different atmospheres is crucial.

Although the 17 - 4 PH SS are widely known for having excellent corrosion resistance, these alloys can suffer with pitting corrosion, which is a localized corrosion caused by local dissolution of the passive film, affecting all properties of the material. This phenomenon is directly related to the presence of pores, that act as liquid channels, facilitating the access of ions into the surface of the material [17, 18]. Furthermore, the formation of oxides on the inner surface of the pores is the likely cause of compositional changes in the periphery of the pores, altering the stability of the passivation films. Lastly, pores can behave like clogged regions of a pit, which can accelerate localized corrosion of the coating, causing catastrophic failures. Based on this, the aim of this work was to investigate the effect of different sintering atmospheres on the porosity and localized corrosion behavior of 17 - 4 PH stainless steel fabricated by MIM process.

2. MATERIALS AND METHODS

The influence of different sintering atmospheres on the localized corrosion properties of two 17 - 4 PH stainless steel samples manufactured by the MIM process in the standard condition of sintering without heat treatment was studied. The first steel samples 17 - 4 PH injected at a temperature of 120°C with molding pressure of 900 bar. They received chemical debiding with nitric acid with a concentration of 99.999% at a temperature of 125°C. After part of the samples were submitted to a sintering process in atmosphere containing 100% N₂ with dew point -30, while another part was sintered in N₂ atmosphere containing 0.2% water vapor with dew point -15 at a temperature of 1350°C.

2.1. Characterization

Concerning the microstructural analysis, all optical images were collected in an Olympus GX51 microscope. The samples were submitted to a compression mounting (Buehler, n° 91-FN-566). The surface of the specimens was ground with abrasive paper from 60# to 1200# and polished with 0.5 and 0.3 μm alumina. The chemical attacks were carried out with Vilela (1g picric acid, 5ml hydrochloric acid and 100ml ethanol) for 300 s. Then, an optical image of each sample was collected at magnification of 50×, to verify the matrix and measure the porosity of the specimens. The porosity was measured using the Thresholding method in ImageJ software. The parameters used in ImageJ were the 8-bit color pattern for better characterization of the pores, discarding of pores that were at the edges of the image selection. In addition, optical images at magnification of 200× were also collected after the electrochemical measurements, aiming to investigate the existence of localized corrosion and pitting. The microhardness of the specimens was evaluated in a Shimadzu HMV-2 microhardness tester 3 measurements were performed in each sample, at random spacing and load of 0.2 kg for 10 s. The chemical composition of the samples was investigated through X-ray energy dispersive spectroscopy (EDX) in a Shimadzu 720 spectrometer.

2.2. Electrochemical measurements

To perform the electrochemical measurements, the samples were embedded in polyester resin and welded to a 15 cm copper wire, grounded ground with abrasive paper in a range of granulometry from 60# to 600# and superficially cleaned with distilled water. Tests were performed in three-electrode configuration, 17 - 4 PH stainless steel as working electrode, platinum as counter electrode and Ag/AgCl (KCl 3M) as reference electrode. A 3.5 wt% NaCl solution was used as an electrolyte. Open circuit measurements were performed for 15 min to determine the open circuit potential (Eco). Electrochemical impedance spectroscopy (EIS) was realized in the range of 1 mHz to 10 KHz, with signal amplitude of 10 mV and 10 points per decade in open circuit potential. For polarization tests, a potentiodynamic scan was performed, starting at 100 mV below the Eco until 0 VAg/AgCl, at scan rate of 1 mV.s-1. All measurements were performed in triplicate, with the specimens grounded and washed between each test.

3. RESULTS AND DISCUSSIONS

The chemical analysis of the samples performed by EDS is described in Table 1. The results are in agreement with the chemical composition of 17 - 4 PH stainless steels reported in the literature. However, it was noted the absence of residual elements such as vanadium (V), manganese (Mn), phosphorus (P), sulfur (S) and silicon (Si). In addition, the lower amount of Mo for both samples (which is normally about 0.23% for 17 - 4 PH stainless steels) may cause a reduction in the ability of passive film to self-regenerate, which can result in lower localized corrosion resistance.

Table 1: Chemical composition of the samples.

	MAJOR CHEMICAL ELEMENTS (%)					
	C	Cr	Cu	Ni	Nb	Mo
Sample 1	0.080	17.427	3.924	3.745	0.252	0.055
Sample 2	0.100	17.557	3.889	4.007	0.301	0.095

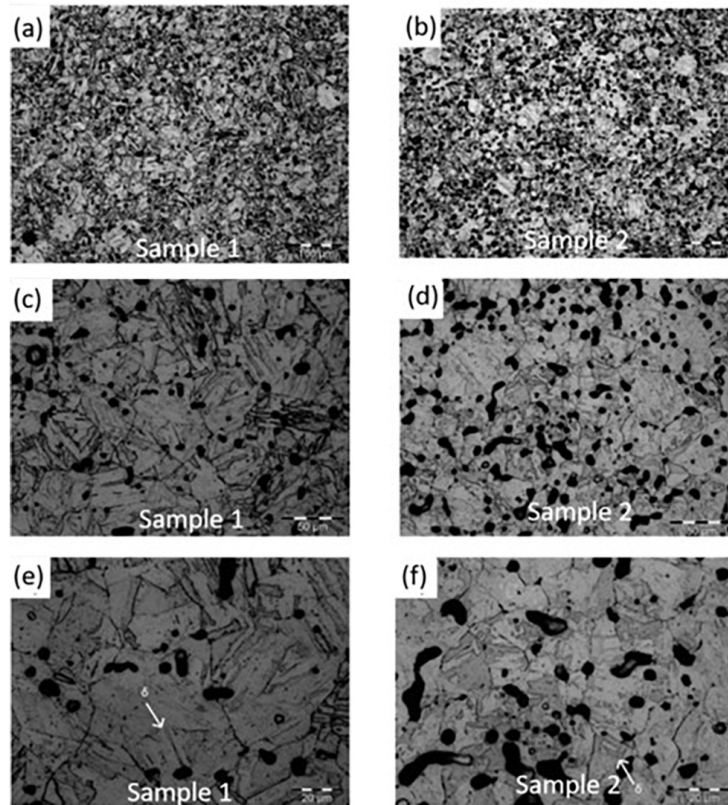


Figure 1: Optical microscopy indicates that sample 1 in Figure 1 (a-c-e) is sintered with pure nitrogen and sample 2 in (b-d-f) is sintered with nitrogen and water vapor.

The optical microscopy images of the samples in different atmospheres and magnifications can be seen in figure 1. The presence of a martensitic matrix and the existence of incoherent copper-based intermetallic precipitates in the different sintering atmospheres. The samples sintered with pure nitrogen can be seen in Figure 1 (a-c-e). Furthermore, a difference in the porosity of samples sintered with nitrogen and water vapor can be clearly seen, with a greater volume of dark spherical areas in figure 1 (b-d-f). The presence of the delta ferrite phase was also observed in both samples.

The microhardness results of the samples are presented in Table 2. Sample 1 (sintered with pure nitrogen) presented an average microhardness of 366 HV (standard deviation of 7.79 HV), while sample 2 (sintered with nitrogen and water vapor) presented a lower value of up to 308 HV (standard deviation of 19.25 HV). It was found that variation in the sintering atmosphere can influence the porosity of the samples and, consequently, the microhardness. However, these values indicated that in the two atmospheres studied, the microhardness found was comparable to that of solubilized 17 - 4 PH steel after sintering [15–18]. The values after sintering are comparable to those found in low alloy steels subjected to quenching and tempering or quenching and partitioning heat treatments [19, 20].

The porosity of the samples was obtained based on the optical images shown in Figure 2, which exhibits the matrix of the samples with no etching. The same area of the images was selected for both samples to obtain more reliable results. The thresholding plugin of Image J was applied and the black spherical regions are

Table 2: Results of microhardness of the samples with Nitrogen (N₂) and Nitrogen-Water.

NITROGEN (N ₂)	MICROHARDNESS HV 1	MAXIMUM STRESS (MPa)
N ₂ - 1	356	1125
N ₂ - 2	367	1169
N ₂ - 3	375	1191
Average	366	1161.7
Standard deviation	7.79	27.44
Nitrogen - Water Vapor (N ₂ - WV)	Microhardness HV 1	Maximum Stress (MPa)
N ₂ - WV -1	334	1048
N ₂ - WV -2	302	950
N ₂ - WV -3	288	915
Average	308	971
Standard deviation	19.25	56.29

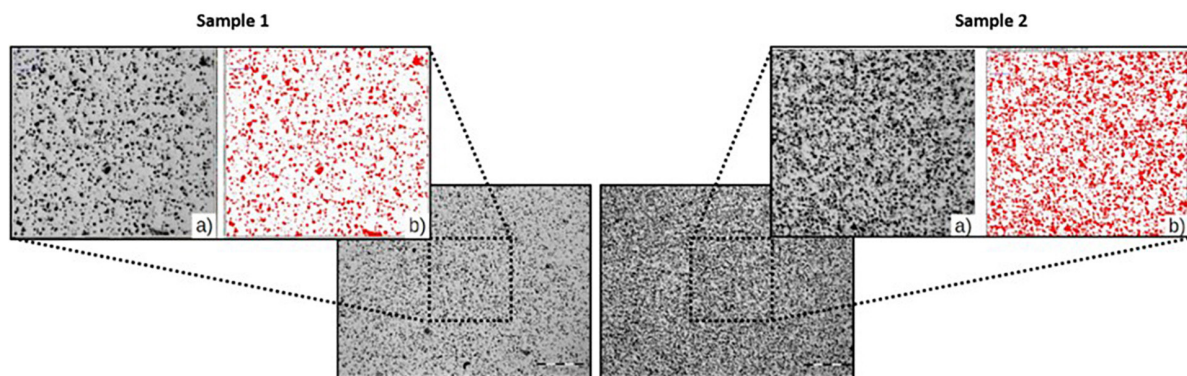


Figure 2: Thresholding plugin of Image J was applied and the black spherical regions.

considered pores and, which after rendering turn to red, as can be seen in Figure 2. Based on these images, the porosity proportion of the samples were calculated, reaching 13.57% and 26.41% for sample 1 and sample 2, respectively. These results suggest a significant influence of the sintering atmosphere on the porosity formation, as observed by the higher volume of pores for the sample produced in an atmosphere containing 99,8% of N₂ and 0,2% of water vapor.

3.1. Electrochemical results

To investigate the electrochemical behavior of the samples, firstly, potentiodynamic polarization test was performed and the results are shown in Figure 3. Comparing the anodic behavior of the samples, it is observed that the corrosion potential of the sample 2 is more active, which is directly associated to its corrosion resistance, suggesting that the material of sample 1 is more noble. In addition, the current density produced by sample 1 was inferior, indicating a higher corrosion rate for sample 2. Furthermore, no passivation behavior was noticed for both samples, which can be due to number of pores acting as active dissolution sites during the test. Thus, it is believed that the dissolution has been concentrated in the pores - which are mostly located in the grain interstices -, consequently, the existing pores have the tendency of increase their size during the tests.

EIS measurements were performed and Figure 3 shows the Nyquist plot for the samples. The experimental data were adjusted through the equivalent circuit shown in Figure 3, which includes the solution resistance (R_s), charge-transfer resistance (R_{ct}), passive film resistance (R_p), and two constant phase elements (CPE₁ and CPE₂). The parameters obtained from the equivalent electric circuit are shown in Table 3. The R_{ct} of sample 1 is substantially higher than sample 2, indicating that the transport of electrons is limited in sample 1, thus preventing corrosion from easily starting. The CPE elements, which were applied in the circuit to represent a behavior

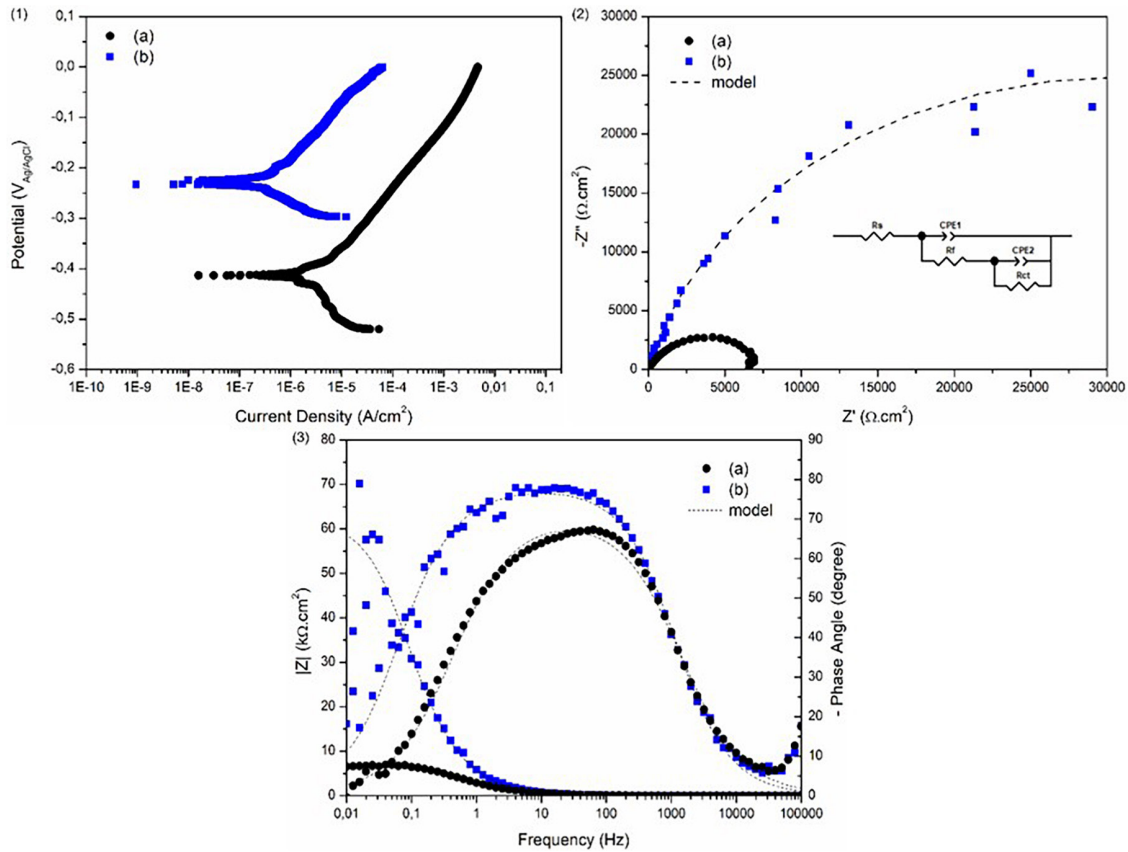


Figure 3: Potentiodynamic polarization curves (1), Nyquist plots (2), and Bode plots (3) for samples sintered with water vapor-based contaminants (a) and pure nitrogen (b).

Table 3: The parameters obtained from the equivalent electric circuit.

Sample	R _s (Ω·cm ²)	R _{ct} (kΩ·cm ²)	CPE ₁ (μs ⁿ ·Ω·cm ⁻²)	n ₁	R _f (Ω·cm ²)	n ₂	CPE ₂ (μs ⁿ ·Ω·cm ⁻²)
MIM-N ₂	12.68	56.60	33.68	0.93	150.17	0.87	41.50
MIM-N ₂ -WV	13.10	6.73	0.02	0.98	11.90	0.54	59.49

between a capacitor and a Warburg element, also presented a difference in their values. The parameter $n = 1$ represents an ideal capacitor, while $n = 0.5$ is related to a Warburg element. It can be observed that the n_2 of sample 2 is equal to 0.54, which is related to the diffusion of the material due to the existence of corrosion reactions, such as the oxidation of Fe to Fe²⁺ and Cr to Cr³⁺, and the reduction of O₂ to OH⁻ or H⁺ to H₂ in localized areas. Furthermore, the R_f values imply that the passive film of sample 1 is more resistant to the formation of localized corrosion. Additionally, at low frequencies, the impedance modulus for sample 1 is significantly higher (around 60 kΩ·cm²) compared to sample 2 (around 6 kΩ·cm²), indicating better corrosion resistance for sample 1.

To investigate the microstructure of the samples after the electrochemical tests, optical images were obtained, as shown in Figure 4. Both samples showed active dissolution sites, confirming the existence of corrosive behavior. As porosity acts as a stress concentrator and accelerates the corrosion process, a difference in pore size can be observed when comparing the samples. Furthermore, as sample 2 had more pores, it is natural that, after the test, they would increase in size in relation to sample 1. It was also considered that sample 2 also had a lower resistance to polarization, higher current density and greater dissolution rate, it is notable that porosity is a crucial factor in the electrochemical behavior of samples. Therefore, corrosion resistance is fully associated with the sintering atmospheres used during sample production. The factor related to the contaminant in the sintering atmosphere contributes to the impairment of surface densification, causing a greater volume of surface porosity [9, 10].

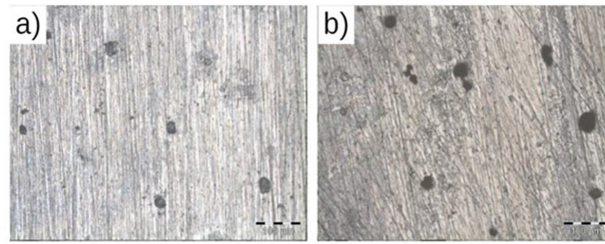


Figure 4: The microstructure of the samples after the electrochemical tests. In (a) sample sintered with pure nitrogen and in (b) with contaminant.

In order to reduce the porosity level of samples sintered with contaminants, it is necessary to use higher temperatures than conventional ones, but this may compromise the metallurgical properties of the final products [9, 10, 21, 22].

4. CONCLUSIONS

From the results and discussions, it is concluded that:

The microstructure of the substrate in both applied sintering atmospheres consists of a martensitic matrix and homogeneously distributed intermetallics.

Samples sintered with the presence of contaminant water vapor showed a higher level of porosity. The presence of delta ferrite was detected in the substrate of samples sintered in both atmospheres. The average microhardness and resistance limit values were higher in samples sintered with pure nitrogen with lower dew point values.

The current density of the sample sintered with pure nitrogen is lower than that detected in the samples sintered with nitrogen and water vapor. Consequently, the corrosion resistance of the sample sintered with nitrogen is greater.

Comparing the anodic behavior of the samples, it is observed that the corrosion potential of the samples sintered in the N_2 condition with water vapor is more active, which is directly associated with its corrosion resistance to resistance, indicating that the material sintered with N_2 is more noble.

The current density of Catamold 17 - 4 PH steel sintered with nitrogen is higher than that of sintering with pure hydrogen found in the literature. Consequently, the hydrogen reducing atmosphere represents the state of the art for the sintering of sintered Catamold 17 - 4 PH steel.

5. BIBLIOGRAPHY

- [1] SUN, Y., HEBERT, R.J., AINDOW, M., “Non-metallic inclusions in 17-4PH stainless steel parts produced by selective laser melting”, *Materials & Design*, v. 140, pp. 153–162, 2018. doi: <http://doi.org/10.1016/j.matdes.2017.11.063>.
- [2] NEZHARDFAR, P.D., SHRESTHA, R., PHAN, N., *et al.*, “Fatigue behavior of additively manufactured 17-4 PH stainless steel: synergistic effects of surface roughness and heat treatment”, *International Journal of Fatigue*, v. 124, pp. 188–204, 2019. doi: <http://doi.org/10.1016/j.ijfatigue.2019.02.039>.
- [3] YU, Z., ZHENG, Y., CHEN, J., *et al.*, “Effect of laser remelting processing on microstructure and mechanical properties of 17-4 PH stainless steel during laser direct metal deposition”, *Journal of Materials Processing Technology*, v. 284, pp. 116738, 2020. doi: <https://doi.org/10.1016/j.jmatprotec.2020.116738>.
- [4] MOYLE, M.S., HAGHDADI, N., LIAO, X.Z., *et al.*, “On the microstructure and texture evolution in 17-4 PH stainless steel during laser powder bed fusion: towards textural design”, *Journal of Materials Science & Technology*, v. 117, p. 183–195, 2022. doi: <https://doi.org/10.1016/j.jmst.2021.12.015>.
- [5] HENRY, T.C., MORALE, M.A., COLE, D.P., *et al.*, “Mechanical behavior of 17-4 PH stainless steel processed by atomic diffusion additive manufacturing”, *International Journal of Advanced Manufacturing Technology*, v. 114, n. 7-8, pp. 20103–20114, 2021. doi: <http://doi.org/10.1007/s00170-021-06785-1>.
- [6] GONÇALVES, R.V., MEDEIROS, J.L.B., BIEHL, L.V., *et al.*, “Aplicação de soluções poliméricas na têmpera do aço inoxidável 17 4 PH solubilizado”, *Matéria (Rio de Janeiro)*, v. 27, n. 2, pp. e202147233, 2022. doi: <http://doi.org/10.1590/1517-7076-rmat-2021-47233>.

- [7] GUO, D., CHEN, J., SHI, Q., *et al.*, “Pitting corrosion behavior of friction-surfaced 17-4PH stainless steel coatings with and without subsequent heat treatment”, *Corrosion Science*, v. 193, pp. 109887, 2021. doi: <https://doi.org/10.1016/j.corsci.2021.109887>.
- [8] BRAZ MEDEIROS, J.L., REGULY, A., STROHACKER, T.R., “Applying oxy-nitrocarburizing surface strengthening process to corrosion prevention in MIM 17-4 PH stainless steel”, *Revista Espacios*, v. 36, n. 20, pp. 21–26, 2015.
- [9] HEANEY, D., “Powders for metal injection molding (MIM)”, In: Heaney, D.F. (ed), *Handbook of Metal Injection Molding MIM*. Sawston, Woodhead Publishing, pp. 45–56, 2019. Woodhead Publishing Series in Metals and Surface Engineering. doi: <http://doi.org/10.1016/B978-0-08-102152-1.00004-0>.
- [10] ENNETI, R.K., ONBATTUVELLI, V.P., ATRE, S.V., “Powder-binder formulation and compound manufacture in metal injection molding (MIM)”, In: Heaney, D.F. (ed), *Handbook of Metal Injection Molding MIM*, Sawston, Woodhead Publishing, pp. 57–88, 2019.
- [11] SCHENEIDER, T.H., BIEHL, L.V., DAS NEVES, E.B., “Method for the determination of parameters in the sintering process of mixtures of the elemental powders Fe-Cr and Fe-Cr-Ni”, *MethodsX*, v. 6, pp. 1919–1924, 2019. doi: <http://doi.org/10.1016/j.mex.2019.08.009>. PubMed PMID: 31516848.
- [12] RIBEIRO, R.B., SOUZA, J.D., BELUCO, A., *et al.*, “Application of the single-minute exchange of die system to the CNC sector of a shoe mold company”, *Cogent Engineering*, v. 6, pp. 1606376, 2019. doi: <http://doi.org/10.1080/23311916.2019.1606376>.
- [13] OLIVEIRA, M.U., BIEHL, L.V., MEDEIROS, J.L., *et al.*, “Manufacturing against corrosion: increasing materials performance by the combination of cold work and heat treatment for 6063 aluminium alloy”, *Medziagotyra*, v. 26, n. 1, pp. 30–33, 2019. doi: <http://doi.org/10.5755/j01.ms.26.1.17683>.
- [14] TAVARES, S.S.M., SILVA, F.J.D., *et al.*, “Microstructure and intergranular corrosion resistance of UNS S17400 (17-4PH) stainless steel”, *Corrosion Science*, v. 52, n. 11, pp. 3835–3839, 2010. doi: <http://doi.org/10.1016/j.corsci.2010.07.016>.
- [15] VIEIRA, E.D.R., BIEHL, L.V., MEDEIROS, J.L.B., *et al.*, “Evaluation of the characteristics of an AISI 1045 steel quenched in different concentration of polymer solutions of polyvinylpyrrolidone”, *Scientific Reports*, v. 11, n. 1, pp. 1313, 2021. doi: <http://doi.org/10.1038/s41598-020-79060-0>. PubMed PMID: 33446669.
- [16] BARROX, A., DOCCOMUN, N., NIVET, E., *et al.*, “Pitting corrosion of 17-4PH stainless steel manufactured by laser beam melting”, *Corrosion Science*, v. 169, pp. 108594, 2020. doi: <https://doi.org/10.1016/j.corsci.2020.108594>.
- [17] LASHGARI, H.R., XUE, Y., ONGGOWARSITO, C., *et al.*, “Microstructure, tribological properties and corrosion behaviour of additively manufactured 17-4PH stainless steel: effects of scanning pattern, build orientation, and single vs. double scan”, *Materials Today*, v. 25, pp. 101535, 2020. doi: <https://doi.org/10.1016/j.mtcomm.2020.101535>.
- [18] LASHGAR, H.R., ADABIFIROOZJAEI, E., KONG, C., *et al.*, “Heat treatment response of additively manufactured 17-4PH stainless steel”, *Materials Characterization*, v. 197, pp. 112661, 2023. doi: <https://doi.org/10.1016/j.matchar.2023.112661>.
- [19] MOTTA, C.A.O.D., SOUZA, J.D., MARTINS, V., *et al.*, “Enhancing composite materials through fly ash reinforcement in powder metallurgy”, *Materials Chemistry and Physics*, v. 307, pp. 128124–128132, 2023. doi: <http://doi.org/10.1016/j.matchemphys.2023.128124>.
- [20] OLIVEIRA, R.C.L.M., BIEHL, L.V., MEDEIROS, J.L.B., *et al.*, “Comparative analysis between quenching and partitioning versus quenching and tempering for SAE 4340”, *Matéria (Rio de Janeiro)*, v. 24, pp. e-12472, 2019. doi: <https://doi.org/10.1590/S1517-707620190003.0788>.
- [21] VIEIRA, E.R., BIEHL, L.V., MEDEIROS, J.L.B., “Effects of the variation of the concentration of aqueous polymer solution based on PVP in the quenching of AISI 4140 steel”, *Matéria (Rio de Janeiro)*, v. 24, pp. e-12425, 2019. doi: <https://doi.org/10.1590/S1517-707620190003.0740>.
- [22] TOCHETTO, R., TOCHETTO, R., BIEHL, L.V., *et al.*, “Evaluation of the space holders technique applied in powder metallurgy process in the use of titanium as biomaterial”, *Latin American Applied Research*, v. 49, n. 4, pp. 261–268, 2019. doi: <http://doi.org/10.52292/j.laar.2019.65>.